Facile E−E and E−C Bond Activation of PhEEPh (E = Te, Se, S) by Ruthenium Carbonyl Clusters: Formation of Di- and Triruthenium Complexes Bearing Bridging dppm and Phenylchalcogenide and Capping Chalcogenido Ligands

Noorjahan Begum,[†] Md. Iqbal Hyder,[†] Mohammad R. Hassan,[†] Shariff E. Kabir,*[,†] Dennis W. Bennett,[‡] Daniel T. Haworth,[‡] Tasneem A. Siddiquee,[‡] Dalia Rokhsana,[§] Ayesha Sharmin,[§] and Edward Rosenberg*[,§]

Department of Chemistry, Jahangirnagar University, Savar, Dhaka 1342, Bangladesh, Department of Chemistry, University of Wisconsin-Milwaukee, Milwaukee, Wisconsin 53211, and Department of Chemistry, The University of Montana, Missoula, Montana 59812

Received October 17, 2007

Reactions of $[Ru_3(CO)_{10}(\mu\text{-dppm})]$ (**1**) and its ortho-metalated derivative $[Ru_3(CO)_9\{\mu_3\text{-}\eta^3\text{-}P(C_6H_5)CH_2P(C_6H_5)(C_6H_4)\}]$ (**11**) with PhEEPh (E = Te, Se, S) have been investigated. Treatment of **1** with PhTeTePh at room temperature afforded the dinuclear compound $[Ru_2(CO)_4(\mu\text{-TePh})_2(\mu\text{-dppm})]$ (**2**) and the 54-electron triruthenium compounds $[Ru_3(CO)_6(\mu_3\text{-Te})_2(\mu\text{-TePh})_2(\mu\text{-dppm})]$ (**3**) and $[Ru_3(CO)_6(\mu_3\text{-Te})(\mu\text{-TePh})_3(\eta^1\text{-COPh})(\mu\text{-dppm})]$ (**4**). Analogous reactions of **1** with PhEEPh (E = Se, S) led to $[Ru_2(CO)_4(\mu\text{-EP}[Ru_3(CO)_6(\mu_3\text{-E})_2(\mu\text{-EPh})_2(\mu\text{-dppm})])_2(\mu\text{-dppm})]$ (E = Se, **5**; E = S, **8**) and the 54-electron triruthenium compounds (E = Se, **6**; E = S, **9**), and $[Ru_3(CO)_6(\mu_3\text{-E})(\mu\text{-EPh})_3(Ph)(\mu\text{-dppm})]$ (E = Se, **7**; E = S, **10**). Reactions of the ortho-metalated complex **11** with PhEEPh (E = Te, Se, S) in refluxing THF gave exclusively $[Ru_3(CO)_6(\mu\text{-EPh})_2\{\mu_3\text{-}\eta^3\text{-}P(C_6H_5)CH_2P(C_6H_5)(C_6H_4)\}]$ (E = Te, **12**; E = Se, **13**; E = S, **14**). The new compounds have been characterized by a combination of analytical and spectroscopic methods, and molecular structures of **2**−**4**, **7**, **10**, and **13** have been determined by single-crystal X-ray diffraction studies. Compounds **2**, **5**, and **8** have the classical "sawhorse" structure with two bridging EPh (E = Te, Se, S) moieties and one bridging dppm ligand. Compounds **3**, **6**, and **9** contain a Ru_3 framework with two bridging EPh (E = Te, Se, S) groups, one bridging dppm ligand, and two capping chalcogenido ligands. Compound **4** contains an Ru_3 core with a capping tellurido ligand, three bridging TePh moieties, one bridging dppm ligand, and a terminally coordinated benzoyl group, formed from multiple fragmentation of the PhTeTePh ligand and migratory insertion of a Ph group into a CO ligand. Compounds **7** and **10** comprise a capping chalcogenido ligand, three bridging EPh (E = Se, **7**; E = S, **10**) moieties, a bridging dppm ligand, and a terminally coordinated σ-bonded phenyl group. In compounds **12**–**14**, the coordination of ortho-metalated diphosphine ligand is the same as in **11** and both the EPh moieties bridge the same unbridged Ru−Ru edge. Compounds **3**, **6**, **7**, and **10** exhibit restricted fluxional behavior involving the μ-EPh moieties.

Introduction

Transition-metal–carbonyl compounds containing chalcogen atoms have attracted much attention in recent years, owing to their importance in fundamental research as well as in technological fields.[1–3] The presence of chalcogen atoms appears to often be decisive in cluster aggregation and condensation reactions.[4–10] In addition, interest in chalcogen-rich metal compounds stems from their unusual structural and reactivity patterns and application as precursors for new solid-state materials.[11,12] A potential route to prepare the chalcogenide carbonyl species is by the facile oxidative addition of $Ph_3P{=}E$ (E = S, Se, Te) to zerovalent metal centers, which commonly generates tertiary phosphine substituted clusters with capping chalcogenide elements.[13] Another method for the synthesis of bridging chalcogenide metal–carbonyl clusters involves the cleavage of E−E bonds of diphenyl dichalcogenide ligands.[14] Applying this latter approach, Lewis et al.[15] and Arce et al.[16] synthesized the 50-electron cluster $[Os_3(CO)_{10}(\mu\text{-SePh})_2]$, in which one SePh group bridged an Os−Os edge and the other an open Os−Os edge, from the reactions of $[Os_3(CO)_{12\text{-}n}(NCMe)_n]$ with PhSeSePh. Recently, Leong and Zhang[17] reported the corresponding tellurium analogue $[Os_3(CO)_{10}(\mu\text{-TePh})_2]$ from the reaction between $[Os_3(CO)_{10}(MeCN)_2]$ and PhTeTePh. Thermolysis of both $[Os_3(CO)_{10}(\mu\text{-SePh})_2]$ and $[Os_3(CO)_{10}(\mu\text{-TePh})_2]$ at 80 °C was reported to lead to an isomer in which both of the EPh (E = Se, Te) moieties bridge the same

* To whom correspondence should be addressed. E-mail: edward.rosenberg@mso.umt.edu (E.R.); skabir_ju@ yahoo.com (S.E.K.).
[†] Jahangirnagar University.
[‡] University of Wisconsin-Milwaukee.
[§] The University of Montana.

(1) (a) Mathur, P.; Philip, R.; Kumar, G. R.; Ghose, S. *Opt. Commun.* **2000**, *178*, 469. (b) Pushkarevsky, N. A.; Bashirov, D. A.; Terenteva, T. G.; Virovets, A. V.; Peresypkina, E. V.; Krautscheid, H.; Konchenko, S. N. *Russ. J. Coord. Chem.* **2006**, *32*, 416. (c) McDonough, J. E.; Weir, J. J.; Sukcharoenphon, K.; Hoff, C. D.; Kryatova, O. P.; Rybak Akimova, E. V.; Scott, B. L.; Kubas, G. J.; Mendiratta, A.; Cummins, C. C. *J. Am. Chem. Soc.* **2006**, *128*, 10295. (d) Henkel, G.; Weissgraber, S. In *Metal Clusters in Chemistry*; Braunstein, P., Oro, L. A., Raithby, P. R., Eds.; Wiley-VCH: Weinheim, Germany, 1999; Vol. 1, p 163. (e) Casado, M. A.; Ciriano, M. A.; Edwards, A. J.; Fernando, J. L.; Perez-Torrente, J. J.; Oro, L. A. *Organometallics* **1998**, *17*, 3414.

10.1021/om701042s CCC: $40.75
Publication on Web 03/05/2008

Chart 1

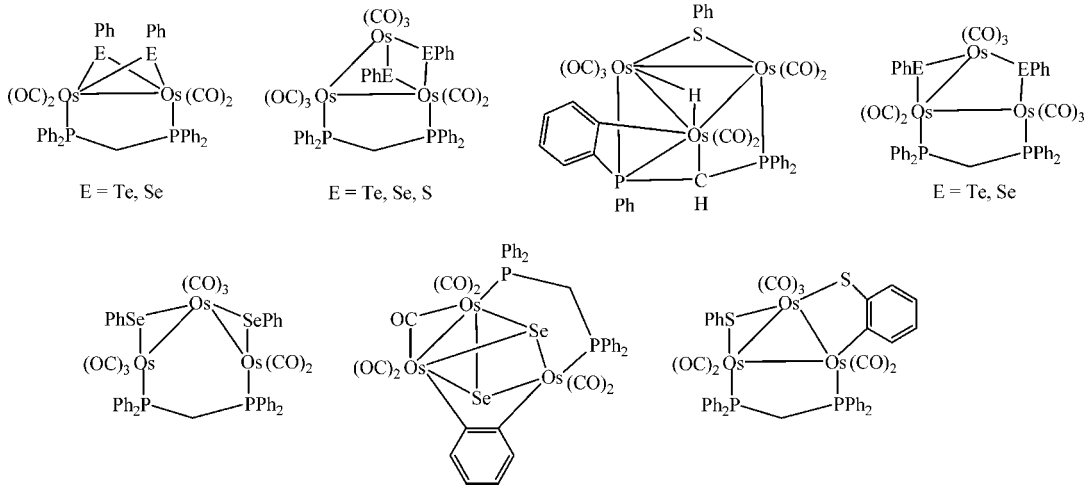

open metal−metal edge. The reactions of the dppm derivative $[Os_3(CO)_{10}(\mu\text{-dppm})]$ with PhEEPh (E = Se, S, Te) resulted in a wide variety of structures, depending on the ligand. For example, the reaction of $[Os_3(CO)_{10}(\mu\text{-dppm})]$ with PhSeSePh at 110 °C afforded the dinuclear compound $[Os_2(CO)_4(\mu\text{-SePh})_2(\mu\text{-dppm})]$, three 50-electron isomeric compounds with the formula $[Os_3(CO)_8(\mu\text{-SePh})_2(\mu\text{-dppm})]$, and the benzyne compound $[Os_3(CO)_6(\mu\text{-CO})(\mu\text{-Se})_2(\mu\text{-}C_6H_4)(\mu\text{-dppm})]$,[18] whereas the corresponding reaction with PhSSPh furnished the three trinuclear compounds $[Os_3(CO)_7(\mu\text{-SPh})(\mu_3\text{-}\eta^4\text{-}Ph_2PCH(Ph)\text{-}C_6H_4)(\mu\text{-H})]$, $[Os_3(CO)_8(\mu\text{-SPh})_2(\mu\text{-dppm})]$, and $[Os_3(CO)_7(\mu\text{-SPh})(\mu\text{-}\eta^2\text{-}SC_6H_4)(\mu\text{-dppm})(\mu\text{-H})]$[19] (Chart 1). In contrast, a similar reaction of $[Os_3(CO)_{10}(\mu\text{-dppm})]$ with PhTeTePh gave the binuclear compound $[Os_2(CO)_4(\mu\text{-TePh})_2(\mu\text{-dppm})]$ and two 50-electron isomeric compounds with the formula $[Os_3(CO)_8(\mu\text{-TePh})_2(\mu\text{-dppm})]$[19] (Chart 1).

To date, only a few examples of the reactivity of $[Ru_3(CO)_{12}]$ with diphenyl dichalcogenides are known. The first report was apparently that involving the reactions of $[Ru_3(CO)_{12}]$ with PhEEPh (E = Te, Se), from which were isolated the dinuclear $[Ru_2(CO)_6(\mu\text{-EPh})_2]$ and the polymeric compounds $[Ru(CO)_2(\mu\text{-EPh})]_n$, whose structures were based on spectroscopic data only.[20] The second report demonstrates the coordination of SePh units on ruthenium carbide carbonyl clusters, affording $[Ru_6C(CO)_{14}(\mu\text{-SePh})_2]$ and other related derivatives.[21] Another recent report describes the synthesis of the dinuclear compound $[Ru_2(CO)_6(\mu\text{-TeC}_6H_4OEt\text{-}4)_2(\mu\text{-dppm})]$ and $[Ru_4(CO)_8(\mu\text{-CO})(\mu_4\text{-Te})_2(\mu\text{-dppm})]$ from the reaction of $[Ru_3(CO)_{10}(\mu\text{-dppm})]$ (**1**) with $Te_2(C_6H_4OEt\text{-}4)_2$ in refluxing toluene.[22] Given the paucity of information reported on the systematic investigation of the reactivity of diphenyl dichalcogenide ligands toward ruthenium carbonyl clusters and in line with our general interest in the synthesis and reactivity of transition-metal−main-group-element mixed-metal clusters, we have now investigated the reactions of PhEEPh (E = Te, Se, S) with $[Ru_3(CO)_{10}(\mu\text{-dppm})]$ (**1**) and obtained several novel chalcogenide-rich 54-electron ruthenium carbonyl clusters resulting from the multiple fragmentation of the PhTeTePh ligand as well as cleavage of all three Ru−Ru bonds. In order to compare the reactivity of the ortho-metalated compound $[Ru_3(CO)_9\{\mu_3\text{-}\eta^3\text{-}P(C_6H_5)CH_2P(C_6H_5)(C_6H_4)\}]$ (**11**) with that of the parent **1**, we have also investigated the reactions of **11** with PhEEPh (E = Te, Se, S) and observed a significantly

(2) Braunstein, P.; Graiff, C.; Massera, C.; Predieri, G.; Rose, J.; Tiripicchio, A. *Inorg. Chem.* **2002**, *41*, 1372.
(3) Shieh, M.; Chen, H.-S.; Lai, Y.-W. *Organometallics* **2004**, *23*, 4018.
(4) Pergola, R. D.; Ceriotti, A.; Cinquantini, A.; de Biani, F. F.; Garlaschelli, L.; Manassero, M.; Piacentini, R.; Sansoni, M.; Zanello, P. *Organometallics* **1998**, *17*, 802.
(5) (a) Dance, I.; Fischer, K. *Inorg. Chem.* **1994**, *41*, 637. (b) Kurakata, H.; Izumi, Y.; Aika, K. *J. Chem. Soc., Chem. Commun.* **1996**, 389. (c) Steigerwald, M. L.; Stuczysnki, S. M.; Kown, Y.-U.; Vennos, D. A.; Brennan, J. G. *Inorg. Chim. Acta* **1993**, *212*, 219. (d) Kuhlman, M. L.; Rauchfuss, T. B. *Organometallics* **2004**, *23*, 5085. (e) Shieh, M.; Hsu, M.-H. *J. Cluster Sci.* **2004**, *15*, 91.
(6) (a) Adams, R. D.; Tasi, M. *J. Cluster Sci.* **1990**, *1*, 249. (b) Adams, R. D. *Polyhedron* **1985**, *4*, 2003. (c) Adams, R. D.; Horvath, I. T. *J. Am. Chem. Soc.* **1984**, *106*, 1869.
(7) Kabir, S. E.; Pervin, S.; Sarker, N. C.; Yesmin., A.; Sharmin, A.; Siddiquee, T. A.; Haworth, D. T.; Bennett, D. W.; Malik, K. M. A. *J. Organomet. Chem.* **2003**, *681*, 237.
(8) Akter, T.; Begum, N.; Yesmin, A.; Haworth, D. T.; Bennett, D. W.; Kabir, S. E.; Miah, Md. A.; Sarker, N. C.; Siddiquee, T. A.; Rosenberg, E. *J. Organomet. Chem.* **2004**, *689*, 237.
(9) (a) Cauzzi, D.; Graiff, C.; Massera, C.; Mori, G.; Predieri, G.; Tiripicchio, A. *J. Chem. Soc., Dalton Trans.* **1998**, 321. (b) Cauzzi, D.; Graiff, C.; Predieri, G.; Tiripicchio, A.; Vignali, C. *J. Chem. Soc., Dalton Trans.* **1999**, 237.
(10) Haung, K. C.; Shieh, M.-H.; Jang, R.-J.; Peng, G.-H.; Lee, G.-H.; Shieh, M. *Organometallics* **1998**, *17*, 1998.
(11) (a) Ansari, M. A.; Ibers, J. A. *Coord. Chem. Rev.* **1990**, *100*, 223. (b) Roof, L. C.; Kolis, J. W. *Chem. Rev.* **1993**, *93*, 1037. (c) Kanatzidis, M. G.; Huang, S. P. *Coord. Chem. Rev.* **1994**, *130*, 223.
(12) (a) Mathur, P.; Thimmappa, B. H. S.; Rheingold, A. L. *Inorg. Chem.* **1990**, *29*, 4658 and references therein. (b) Mathur, P.; Reddy, V. D.; Das, K.; Sinha, U. C. *J. Organomet. Chem.* **1991**, *409*, 255 and references therein. (c) Bogan, L. E., Jr.; Lesch, D. A.; Rauchfuss, T. B. *J. Organomet. Chem.* **1983**, *250*, 429. (d) Roof, L. C.; Pennington, W. T.; Kolis, J. W. *J. Am. Chem. Soc.* **1990**, *112*, 8172.
(13) (a) Cauzzi, D.; Graiff, C.; Predieri, G.; Tiripicchio, A. *Metal Clusters in Chemistry*; Baistrocchi P., Oro L. A., Raithby P. R., Tiripicchio A., Eds.; VCH: Weinheim, Germany, 1999; Vol. 1, pp 193–208. (b) Leong, W. K.; Leong, W. L. J.; Zhang, J. *J. Chem. Soc., Dalton Trans.* **2001**, 1087. (c) Ahmed, S. J.; Hyder, Md. I.; Kabir, S. E.; Miah, Md. A.; Deeming, A. J.; Nordlander, E. *J. Organomet. Chem.* **2006**, *691*, 309.
(14) Sadekov, I. D.; Uraev, A. I.; Garnovskii, A. D. *Russ. Chem. Rev.* **1999**, *68*, 415.
(15) Broadhurst, P. V.; Johnson, B. F. G.; Lewis, J. *J. Chem. Soc., Dalton Trans.* **1982**, 1881.
(16) (a) Arce, A. J.; Arrojo, P.; Sanctis, Y. De.; Deeming, A. J.; West, D. J. *Polyhedron* **1992**, *11*, 1013. (b) Arce, A. J.; Arrojo, P.; De Sanctis, Y.; Deeming, A. J. *J. Chem. Soc, Chem. Commun.* **1991**, 1491.
(17) Zhang, J.; Leong, W. K. *Dalton Trans.* **2000**, 1279.
(18) Kabir, S. E.; Begum, N.; Hassan, Md. M.; Hyder, Md. I.; Nur, H.; Bennett, D. W.; Siddiquee, T. A.; Haworth, D. T.; Rosenberg, E. *J. Organomet. Chem.* **2004**, *689*, 1569.
(19) Kabir, S. E.; Saha, M. S.; Tocher, D. A.; Hossain, G. M. G.; Rosenberg, E. *J. Organomet. Chem.* **2006**, *691*, 97.
(20) Schermer, E. D.; Baddley, W. H. *J. Organomet. Chem.* **1971**, *30*, 67.
(21) Chihara, T.; Yamazaki, H. *J. Organomet. Chem.* **1992**, *428*, 169.
(22) Azam, K. A.; Bhowmick, M.; Hossain, G. M. G.; Kabir, S. E.; Kundu, K.; Malik, K. M. A.; Perven, S. *J. Chem. Crystallogr.* **2001**, *31*, 63.

Scheme 1

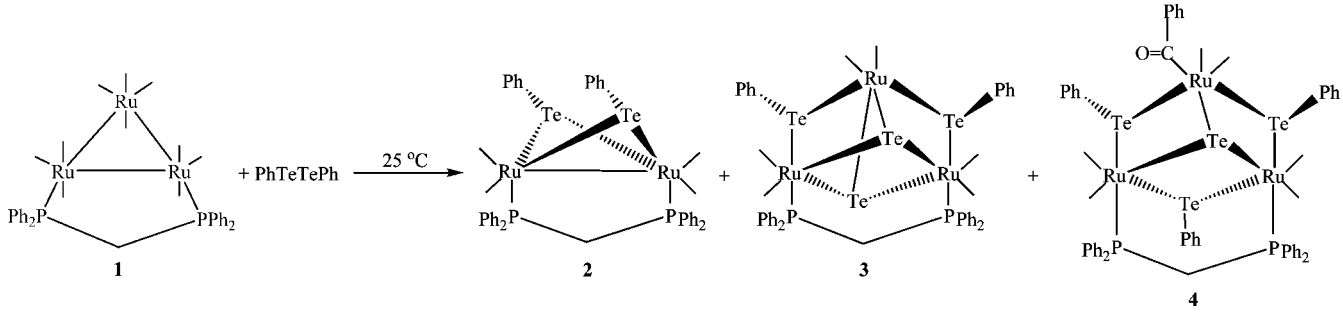

different reactivity leading to the formation of the 48-electron clusters $[Ru_3(CO)_6(\mu\text{-EPh})_2\{\mu_3\text{-}\eta^3\text{-P}(C_6H_5)CH_2P(C_6H_5)(C_6H_4)\}]$.

Results and Discussion

Reaction of $[Ru_3(CO)_{10}(\mu\text{-dppm})]$ (1) with PhTeTePh. The reaction of **1** with PhTeTePh at 25 °C, followed by thin-layer chromatographic separation, furnished the binuclear compound $[Ru_2(CO)_4(\mu\text{-TePh})_2(\mu\text{-dppm})]$ (**2**) and the trinuclear compounds $[Ru_3(CO)_6(\mu_3\text{-Te})_2(\mu\text{-TePh})_2(\mu\text{-dppm})]$ (**3**) and $[Ru_3(CO)_6(\mu_3\text{-Te})(\mu\text{-TePh})_3(\eta^1\text{-COPh})(\mu\text{-dppm})]$ (**4**) (Scheme 1) in 14, 18, and 22% yields, respectively. When the reaction was conducted in refluxing THF, the yield of the dinuclear compound **2** was increased slightly but those of the trinuclear compounds **3** and **4** were decreased significantly. All these compounds are stable in the solid state and decompose in solution over period of days. The compounds were characterized by a combination of elemental analysis, IR, ^{1}H NMR, ^{31}P{^{1}H} NMR, mass spectral data, and single-crystal X-ray diffraction studies.

An ORTEP diagram giving the molecular structure of **2** is depicted in Figure 1, crystal data are collected in Table 1, and selected bond distances and angles are listed in the caption to the figure. The basic structure of **2** is comparable to that of $[Ru_2(CO)_4(\mu\text{-TeC}_6H_4OEt\text{-}4)_2(\mu\text{-dppm})]$.[22] The metal core of compound **2** contains a Te_2Ru_2 butterfly geometry with the wingtips of Te atoms linked with two phenyl groups. The ruthenium−ruthenium backbone is ligated by four terminal carbonyl ligands and bridged by a dppm ligand. The TePh and the dppm ligands are transoid to each other, and the Ru−Ru−Te planes are perpendicular to each other. The Ru−Ru bond distance of 2.7475(9) Å is comparable to the corresponding distances in $[Ru_2(CO)_4(\mu\text{-SePh})_2(\mu\text{-dppm})]$ (2.8719(7) Å). The Ru−Te bond distances (Ru(2)−Te(2) = 2.6745(11), Ru(1)−Te(2) = 2.6753(10), Ru(1)−Te(1) = 2.6691(8), Ru(2)−Te(1) = 2.6988(8) Å) are comparable to those observed in $[Ru_2(CO)_4(\mu\text{-SePh})_2(\mu\text{-dppm})]$.[22] The spectroscopic data of **2** are consistent with the solid-state structure. The carbonyl stretching frequencies in the IR spectrum are very similar to those reported for $[Ru_2(CO)_4(\mu\text{-TeC}_6H_4OEt\text{-}4)_2(\mu\text{-dppm})]$.[22] In addition to the phenyl proton resonances of the dppm and TePh moieties in the aromatic region, the ^{1}H NMR spectrum contains two multiplets at δ 4.57 and 2.49 assigned to the methylene protons of the dppm ligand. The two phosphorus nuclei are equivalent, and as expected, the ^{31}P{^{1}H} NMR spectrum of **2** shows a singlet at δ 13.9. The mass spectrum confirms the stoichiometry with a molecular ion peak at *m*/*z* 1108.

An ORTEP diagram of the molecular structure of **3** is shown in Figure 2, crystal data are collected in Table 1, and selected bond distances and angles are listed in the caption to the figure. The molecule consists of three ruthenium atoms arranged in an open fashion with no metal−metal bonds containing one bridging dppm ligand, two bridging TePh groups, two capping telluride ligands, and six terminal carbonyl ligands, two bonded to each ruthenium atom. A striking feature of the structure is the occurrence of one bridging ligand across each open Ru−Ru edge. One TePh ligand asymmetrically bridges the Ru(1)···Ru(3) edge (Ru(1)−Te(3) = 2.7058(19) and Ru(3)−Te(3) = 2.651(2) Å), and the other asymmetrically bridges the Ru(2)···Ru(3) edge (Ru(2)−Te(4) = 2.7110(18) and Ru(3)−Te(3) = 2.652(2) Å). The dppm ligand symmetrically spans the open Ru(1)···Ru(2) edge (Ru(1)−P(1) = 2.340(5) and Ru(2)−P(2) = 2.341(5) Å) and occupies axial coordination sites. The nonbonding Ru···Ru distance associated with the dppm bridge (Ru(1)···Ru(2) = 4.124 Å) is significantly longer than those involving the TePh bridge (Ru(1)···Ru(3) = 3.581, Ru(2)···Ru(3) = 3.582 Å). Another interesting feature is that one tellurido ligand symmetrically caps the three Ru atoms (Ru(3)−Te(1) = 2.7762(19), Ru(2)−Te(1) = 2.7803(18) and Ru(1)−Te(1) = 2.7827(18) Å), while the other ligand asymmetrically caps the Ru_3 system

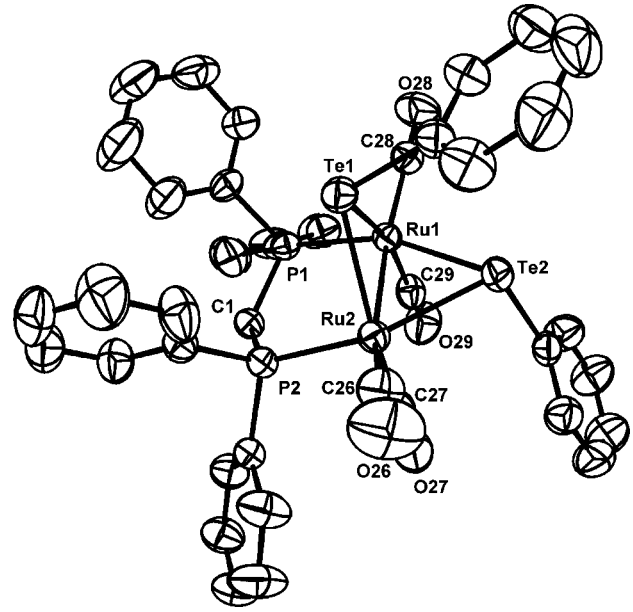

Figure 1. ORTEP diagram of $[Ru_2(CO)_4(\mu\text{-TePh})_2(\mu\text{-dppm})]$ (**2**) with 50% probability thermal ellipsoids. Selected interatomic distances (Å) and angles (deg): Ru(2)−Ru(1) = 2.7475(9), Ru(2)−Te(2) = 2.6745(11), Ru(1)−Te(2) = 2.6753(10), Ru(1)−Te(1) = 2.6691(8), Ru(2)−Te(1) = 2.6988(8), Ru(2)−C(27) = 1.880(7), Ru(2)−C(26) = 1.888(7), Ru(2)−P(2) = 2.3172(17), Ru(1)−C(29) = 1.872(6), Ru(1)−C(28) = 1.894(6), Ru(1)−P(1) = 2.3162(18); Ru(2)−Te(2)−Ru(1) = 61.80(3), Ru(1)−Te(1)−Ru(2) = 61.57(2), P(2)−Ru(2)−Te(2) = 153.47(4), P(2)−Ru(2)−Te(1) = 92.31(4), Te(2)−Ru(2)−Te(1) = 79.88(2), P(2)−Ru(2)−Ru(1) = 95.12(4), Te(2)−Ru(2)−Ru(1) = 59.113(19), Te(1)−Ru(2)−Ru(1) = 58.68(2), Te(1)−Ru(1)−Te(2) = 80.40(2), P(1)−Ru(1)−Ru(2) = 94.17(4), Te(1)−Ru(1)−Ru(2) = 59.747(16), Te(2)−Ru(1)−Ru(2) = 59.08(2), P(2)−C(1)−P(1) = 114.9(3).

Table 1. Crystal Data for Compounds 2−4, 7, 10, and 13

	2	**3**	**4**
empirical formula	$C_{41}H_{32}O_4P_2Ru_2Te_2$	$C_{43}H_{32}O_6P_2Ru_3Te_4$	$C_{56}H_{42}O_7P_2Ru_3Te_4$
fw	1106.71	1517.74	1699.95
temp, K	293(2)	293(2)	293(2)
wavelength (Å)	0.710 73	0.710 73	0.710 73
cryst syst	monoclinic	orthorhombic	monoclinic
space group	$P2_1/2$	*Pbca*	$P2_1/c$
a (Å)	11.015(5)	19.621(5)	14.324(4)
b (Å)	18.542(5)	22.168(5)	20.600(5)
c (Å)	19.843(5)	23.948(5)	20.514(3)
α (deg)	90.000(5)	90.000(5)	90
β (deg)	92.340(5)	90.000(5)	103.01(2)
γ (deg)	90.000(5)	90.000(5)	90
V (Å^3)	4049(2)	10416(4)	5898(2)
Z	4	8	5
calcd density (Mg/m^3)	1.817	2.141	1.917
abs coeff (mm^{-1})	2.276	3.546	2.800
F(000)	2128	6246	3216
cryst size (mm^3)	0.37 × 0.18 × 0.24	0.30 × 0.16 × 0.15	0.44 × 0.13 × 0.13
θ range for data collecn (deg)	2.05−25.01	1.84−24.99	1.76−22.49
index ranges	$-13 \le h \le 1$	$-23 \le h \le 1$	$-1 \le h \le 15$
	$-1 \le k \le 22$	$-21 \le k \le 1$	$-1 \le k \le 22$
	$-23 \le l \le 23$	$-1 \le l \le 23$	$-22 \le l \le 21$
no. of rflns collected	8880	5950	9339
no. of indep rflns	7121 (*R*(int) = 0.0401)	4883 (*R*(int) = 0.0324)	7671 (*R*(int) = 0.0263)
no. of data/restraints/params	7121/0/460	4883/0/523	7671/0/649
goodness of fit on F^2	0.934	1.033	1.062
final *R* indices ($I > 2\sigma(I)$)	R1 = 0.0379	R1 = 0.0529	R1 = 0.0477
	wR2 = 0.0941	wR2 = 0.1332	wR2 = 0.1467
R indices (all data)	R1 = 0.0492	R1 = 0.0821	R1 = 0.0610
	wR2 = 0.1522	wR2 = 0.1559	wR2 = 0.1020
largest diff peak and hole (e Å^{-3})	2.698 and –0.679	1.117 and −0.778	4.994 and –0.781

	7	**10**	**13**
empirical formula	$C_{55}H_{42}O_6P_2Ru_3Se_4$	$C_{55}H_{42}O_6P_2Ru_3S_4$	$C_{37}H_{26}O_6P_2Ru_3Se_2$
fw	1479.88	1517.74	1089.65
temp, K	293(2)	293(2)	293(2)
wavelength (Å)	0.710 73	0.710 73	0.710 73
cryst syst	triclinic	triclinic	triclinic
space group	$P\bar{1}$	$P\bar{1}$	$P2_1/c$
a (Å)	13.103(2)	13.243(5)	13.2641(6)
b (Å)	13.604(2)	13.758(5)	18.3099(8)
c (Å)	17.044(3)	16.578(5)	16.7128(8)
α (deg)	95.790(10)	97.570(5)	90
β (deg)	93.410(10)	91.790(5)	109.9050(10)
γ (deg)	115.750(10)	117.290(5)	90
V (Å^3)	2704.3(7)	2646.4(16)	3816.5(3)
Z	2	2	4
calcd density (Mg/m^3)	1.817	1.448	1.896
abs coeff (mm^{-1})	3.626	1.064	3.207
F(000)	1436	1148	2104
crystal size (mm^3)	0.27 × 0.18 × 0.16	0.19 × 0.17 × 0.06	0.51 × 0.16 × 0.06
θ range for data collecn (deg)	1.80−22.49	1.77−22.37	1.63−28.31
index ranges	$-14 \le h \le 1$	$-1 \le h \le 7$	$-17 \le h \le 17$
	$-12 \le k \le 12$	$-13 \le k \le 12$	$-23 \le k \le 23$
	$-16 \le l \le 16$	$-15 \le l \le 15$	$-22 \le l \le 22$
no. of rflns collected	5986	4624	33 620
no. of indep rflns	5102 (*R*(int) = 0.0484)	3759 (*R*(int) = 0.0274)	9079 (*R*(int) = 0.0357)
no. of data/restraints/params	5102/0/631	3759/36/631	9079/0/451
goodness of fit on F^2	1.059	0.844	0.854
final *R* indices ($I > 2\sigma(I)$)	R1 = 0.0474	R1 = 0.0319	R1 = 0.0362
	wR2 = 0.1049	wR2 = 0.0855	wR2 = 0.0842
R indices (all data)	R1 = 0.0820	R1 = 0.0486	R1 = 0.0525
	wR2 = 0.094	wR2 = 0.0938	wR2 = 0.1205
largest diff peak and hole (e Å^{-3})	0.614 and –0.639	0.340 and −0.386	0.714 and –0.333

(Ru(1)−Te(2) = 2.7675(18), Ru(2)−Te(2) = 2.7639(18), and Ru(3)−Te(2) = 2.7907(19) Å). Overall, compound **3** contains a total of 54 cluster valence electrons, which is precisely the number expected for an open cluster of three metal atoms with each ruthenium atom having an 18-electron configuration.[23] The formulation of the cluster is supported by its FAB mass spectrum, which exhibits a molecular ion peak at *m*/*z* 1522. The $^{31}P\{^1H\}$ NMR spectrum at room temperature displays two singlets at *δ* 14.4 and 13.9, indicating that the molecule exhibits some sort of isomerism in solution (see VT NMR studies section), which is also supported by the ^1H NMR spectrum.

An ORTEP diagram of the molecular structure of **4** is shown in Figure 3, crystal data are given in Table 1, and selected bond distances and angles are collected in the caption to the figure.

(23) Mingos, D. M. P. *Acc. Chem. Res.* **1984**, *17*, 311.

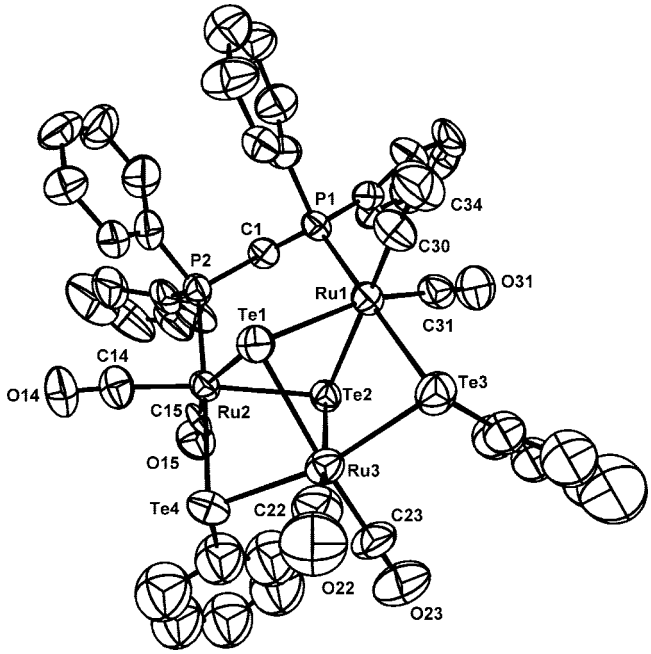

Figure 2. ORTEP diagram of $[Ru_3(CO)_6(\mu_3\text{-}Te)_2(\mu\text{-}TePh)_2(\mu\text{-}dppm)]$ (**3**) with 50% probability thermal ellipsoids. Selected interatomic distances (Å) and angles (deg): Ru(1)···Ru(2) = 4.124, Ru(2)···Ru(3) = 3.582, Ru(1)···Ru(3) = 3.581, Ru(3)−Te(1) = 2.7762(19), Ru(2)−Te(1) = 2.7803(18), Ru(1)−Te(1) = 2.7827(19), Ru(2)−Te(2) = 2.7639(18), Ru(1)−Te(2) = 2.7675(18), Ru(3)−Te(2) = 2.7907(19), Ru(2)−P(2) = 2.341(5), Ru(1)−P(1) = 2.340(5) Ru(2)−Te(4) = 2.7110(18), Ru(1)−Te(3) = 2.7058(19), Ru(3)−Te(4) = 2.655(2), Ru(3)−Te(3) = 2.651(2); Ru(3)−Te(1)−Ru(2) = 80.30(5), Ru(3)−Te(1)−Ru(1) = 80.20(5), Ru(2)−Te(1)−Ru(1) = 95.67(5), Ru(2)−Te(2)−Ru(1) = 96.39(6), Ru(2)−Te(2)−Ru(3) = 80.33(5), Ru(1)−Te(2)−Ru(3) = 80.21(5), Te(4)−Ru(2)−Te(2) = 85.83(5), Te(4)−Ru(2)−Te(1) = 82.74(5), Te(2)−Ru(2)−Te(1) = 75.97(5), Te(3)−Ru(1)−Te(2) = 85.97(5), Te(3)−Ru(1)−Te(1) = 82.66(5), Te(2)−Ru(1)−Te(1) = 75.87(5), Ru(3)−Te(4)−Ru(2) = 83.77(5), Ru(3)−Te(3)−Ru(1) = 83.88(5), Te(3)−Ru(3)−Te(4) = 166.95(7), Te(3)−Ru(3)−Te(1) = 83.78(6), Te(4)−Ru(3)−Te(1) = 83.84(6), Te(3)−Ru(3)−Te(2) = 86.56(5), Te(4)−Ru(3)−Te(2) = 86.37(5), Te(1)−Ru(3)−Te(2) = 75.60(5), P(1)−C(1)−P(2) = 118.5(8).

It is a structurally unique open cluster of three ruthenium atoms with a TePh ligand asymmetrically bridging each of the three nonbonded Ru···Ru edges and a capping telluride ligand. It also contains a diaxially coordinated dppm ligand that symmetrically spans (Ru(1)−P(8) = Ru(6)−P(9) = 2.363(3) Å) one of the Ru(1)···Ru(6) edges, which is simultaneously bridged by a TePh moiety. Each of the ruthenium atoms has two terminal carbonyl ligands. An interesting feature is that the tellurido ligand symmetrically caps the three Ru atoms (Ru(7)−Te(2) = 2.7366(13), Ru(1)−Te(2) = 2.7410(14), Ru(6)−Te(2) = 2.7452(12) Å). The TePh-bridged nonbonded Ru···Ru edges (Ru(6)···Ru(7) = 4.017, Ru(1)···Ru(7) = 4.156 Å) are significantly longer than the corresponding nonbonded edges in **3**. Interestingly, the dppm-bridged Ru(1)···Ru(6) distance (3.991 Å) is shorter than the corresponding distance in **3**. The reason for this shortness is most probably due to the presence of the bridging TePh ligand along the same edge. The Ru−Te bond distances involving the TePh bridges that span from 2.7220(12) to 2.7909(13) Å are in good agreement with those observed in **3**. An intriguing feature of the structure is the η^1 coordination of a benzoyl group to Ru(3), which is formed by insertion of a phenyl group into the C(24)−O(24) carbonyl group. The Ru(3)−C(24) bond distance of 2.080(13) Å and the C(24)−O(24) bond distance of 1.232(15) Å, respectively, are shorter and longer than those observed for the terminally coordinated benzoyl unit in ruthenium compounds.[24] Compound **4** contains a total of 54 cluster valence electrons, as expected for a triruthenium complex with no metal−metal bonds, and each ruthenium atom formally has an 18-electron configuration.[23] The formulation of **4** is confirmed by its FAB mass spectrum, which exhibits the molecular ion peak at *m*/*z* 1704, and the IR spectrum contains an absorption at 1735 cm^{-1} assignable to ν(CO) of the benzoyl moiety. The two phosphorus atoms in **4** are nonequivalent, since the $^{31}P\{^1H\}$ NMR spectrum exhibits two doublets at δ 12.1 and 11.1 with a phosphorus−phosphorus coupling constant of 11.7 Hz, indicating the presence of a single isomer.

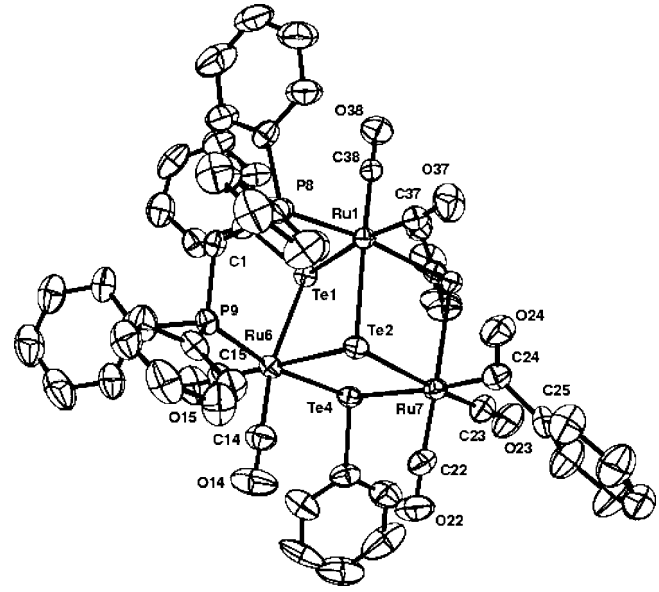

Figure 3. ORTEP diagram of $[Ru_3(CO)_6(\mu_3\text{-}Te)(\mu\text{-}TePh)_3(COPh)(\mu\text{-}dppm)]$ (**4**) with 50% probability thermal ellipsoids. Selected interatomic distances (Å) and angles (deg): Ru(1)···Ru(6) = 3.991, Ru(6)···Ru(7) = 4.017, Ru(1)···Ru(7) = 4.156, Ru(1)−Te(1) = 2.7220(12), Ru(6)−Te(1) = 2.7440(14), Ru(7)−Te(2) = 2.7366(13), Ru(1)−Te(2) = 2.7410(14), Ru(6)−Te(2) = 2.7452(12), Ru(7)−Te(3) = 2.7355(14), Ru(1)−Te(3) = 2.7503(12), Ru(1)−P(8) = 2.363(3), Ru(6)−Te(4) = 2.7412(13), Ru(7)−Te(4) = 2.7909(13), Ru(6)−P(9) = 2.363(3), Ru(7)−C(24) = 2.080(13); P(8)−C(1)−P(9) = 121.0(6), Ru(1)−Te(1)−Ru(6) = 93.81(4), Ru(7)−Te(2)−Ru(1) = 98.69(4), Ru(7)−Te(2)−Ru(6) = 97.06(4), Ru(1)−Te(2)−Ru(6) = 93.36(4), Ru(7)−Te(3)−Ru(1) = 98.49(4), Te(1)−Ru(1)−Te(2) = 83.98(4), P(8)−Ru(1)−Te(3) = 172.14(8), Te(1)−Ru(1)−Te(3) = 86.79(4), Te(2)−Ru(1)−Te(3) = 80.75(4), Ru(6)−Te(4)−Ru(7) = 95.88(4), Te(4)−Ru(6)−Te(1) = 76.00(3), P(9)−Ru(6)−Te(2) = 88.61(8), Te(4)−Ru(6)−Te(2) = 83.67(4), Te(1)−Ru(6)−Te(2) = 83.49(4), Te(3)−Ru(7)−Te(2) = 81.10(3), Te(3)−Ru(7)−Te(4) = 95.57(4), Te(2)−Ru(7)−Te(4) = 82.91(4).

Reactions of $[Ru_3(CO)_{10}(\mu\text{-dppm})]$ (1) with PhSeSePh and PhSSPh. Similar reactions of **1** with PhSeSePh and PhSSPh took a slightly different course, affording the dinuclear compounds $[Ru_2(CO)_4(\mu\text{-}EPh)_2(\mu\text{-dppm})]$ (**5**, E = Se, 11%; **8**, E = S, 15%) and the trinuclear compounds $[Ru_3(CO)_6(\mu_3\text{-}E)_2(\mu\text{-}EPh)_2(\mu\text{-dppm})]$ (**6**, E = Se, 25%; **9**, E = S, 18%) and $[Ru_3(CO)_6(\mu_3\text{-}E)(\mu\text{-}EPh)_3(\eta^1\text{-}Ph)(\mu\text{-dppm})]$ (**7**, E = Se, 35%; **10**, E = S, 14%) (Scheme 2). It is interesting to note that we

(24) R Charmant, J. P. H.; Dickson, H. A. A.; Grist, N. J.; Keister, J. B.; Knox, S. A. R.; Morton, D. A. V.; Orpen, A. G.; Vinas, J. M. *J. Chem. Soc., Chem. Commun.* **1991**, 1393.

Scheme 2

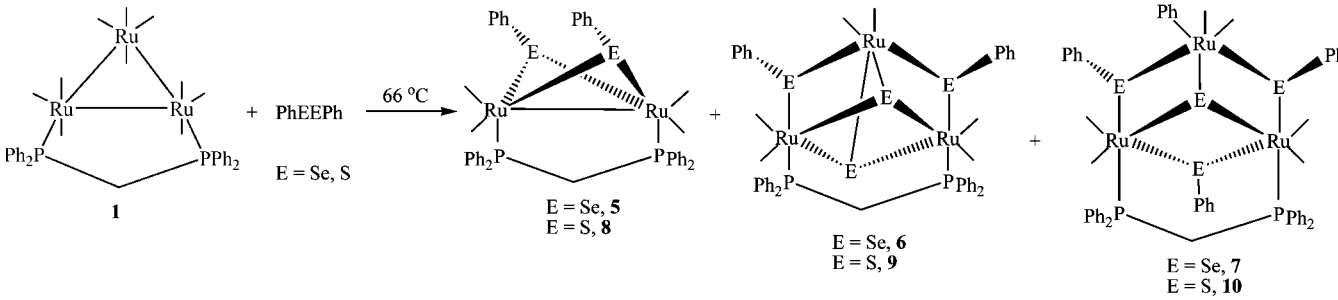

were not able to isolate any benzoyl-coordinated compound analogous to **4**; instead, we obtained the σ-bonded phenyl compounds **7** and **10**. The new compounds were characterized by IR, ^{1}H NMR, ^{31}P{^{1}H} NMR, mass spectral data, and elemental analyses together with single-crystal diffraction studies for **7** and **10**. The carbonyl stretching frequencies in the infrared spectra of **5** and **8** are similar to those of **2**, indicating that they are isostructural. The mass spectra of **5** and **8** show the molecular ion peaks (*m*/*z* 1012 for **5** and 818 for **8**) with successive loss of four carbonyl groups. The ^{31}P{^{1}H} NMR spectra contain a singlet at δ 24.2 for **5** and δ 29.3 for **8**, indicating equivalent ^{31}P nuclei. As expected, the dppm methylene protons show two multiplets at δ 4.42 and 3.87 for **5** and at δ 4.34 and 3.59 for **8**, and these solution data fit a structure similar to that found in **2**. The patterns of the IR spectra of **6** and **9** are similar to that of **3**, indicating a similar distribution of the carbonyl ligands. The mass spectra of **6** and **9** confirm the stoichiometry with ion peaks at *m*/*z* 1326 and 1139. The ^{31}P{^{1}H} NMR spectrum of **3** at room temperature exhibits two singlets δ at 27.8 and 27.4, indicating isomerism similar to that of **6**. The ^{31}P{^{1}H} NMR spectrum of **9** at room temperature exhibits a singlet at δ 27.8, implying a dynamic behavior different from that of **3** and **6** (see Variable-Temperature NMR Studies).

The ORTEP drawings of the molecular structures of **7** and **10** are depicted in Figures 4 and 5, respectively, crystal data are given in Table 1, and selected bond distances and angles are collected in the captions to the figures. Both complexes are open triruthenium clusters with three bridging phenylchalcogenido groups, each bridging across one open Ru···Ru edge, a σ-Ru−C-bonded phenyl group, a bridging dppm, and a capping chalcogenido ligand. Each ruthenium atom has two terminally coordinated CO groups. Compounds **7** and **10** are structurally similar to **4** except in place of a terminally coordinated benzoyl group there are terminally coordinated phenyl groups. The nonbonding Ru−Ru distances in **10** (Ru(1)···Ru(6) = 3.670, Ru(2)···Ru(3) = 3.682, Ru(1)···Ru(3) = 3.723 Å) are significantly shorter than those in **7** (Ru(1)···Ru(2) = 3.843, Ru(2)···Ru(3) = 3.872, Ru(1)···Ru(3) = 3.796 Å), which in turn are significantly shorter than those observed in **4**. The lengthening of all the nonbonded Ru−Ru distances from **10** to **7** to **4** can be attributed to the increase in the size of the bridging atom across these edges. In **7**, the Ru_3 framework is symmetrically capped by the selenido ligand (Ru(1)−Se(1) = 2.5646(16), Ru(2)−Se(1) = 2.5646(16), Ru(3)−Se(1) = 2.5539(16) Å), and in **10**, the Ru_3 core is almost symmetrically capped by the sulfido ligand (Ru(1)−S(4) = 2.428(3), Ru(2)−S(4) = 2.440(2), Ru(3)−S(4) = 2.451(2) Å) with average Ru−Se and Ru−S distances of 2.561(2) and 2.489(2) Å, respectively, which are longer than the corresponding distances in $[Ru_3(CO)_7(\mu_3\text{-}CO)(\mu_3\text{-}Se)(\mu\text{-}dppm)]$ (average 2.4893(4) Å) and $[Ru_3(CO)_7(\mu_3\text{-}CO)(\mu_3\text{-}Se)(\mu\text{-}dppm)]$ (average 2.366(3) Å).[13c] An interesting feature of the structures is the presence of a phenyl group σ-bonded to the Ru atom not bridged by the dppm ligand: Ru(2)−C(50) = 2.125(13) Å for **7** and Ru(3)−C(44) = 2.129(11) Å for **10**. The diaxially coordinated dppm ligand spans the Ru(1)···Ru(3) nonbonded edge in **7** and the Ru(1)···Ru(2) nonbonded edge in **10** with Ru−P distances (Ru(3)−P(1) = 2.351(3), Ru(1)−P(2) = 2.348(3) Å for **7**; Ru(1)−P(1) = 2.344(3), Ru(2)−P(2) = 2.348(3) Å for **10**) comparable to those observed in **1**.[25]

Because of their close structural similarity, the IR spectra of **7** and **10** in the carbonyl region are similar to that of **4**, except that the ν(CO) absorption of the benzoyl moiety observed in **4** is absent in **7** and **10**. The ^{31}P{^{1}H} NMR spectra of **7** and **10**

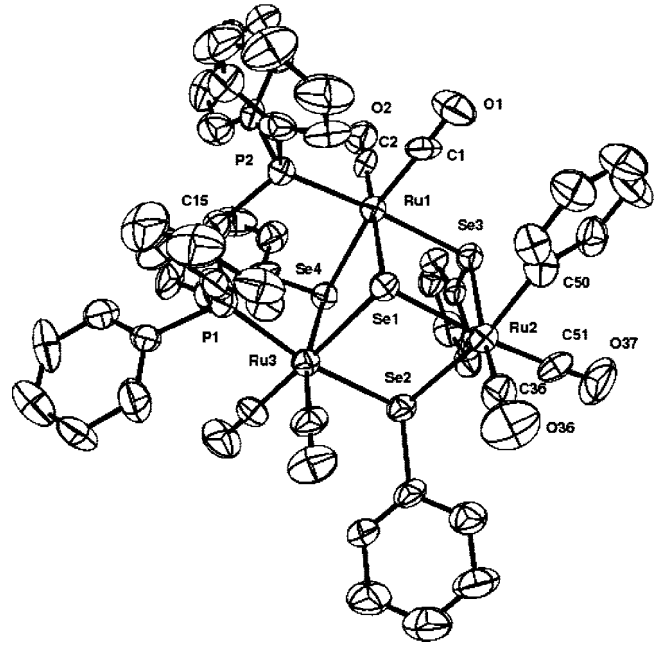

Figure 4. ORTEP diagram of $[Ru_3(CO)_6(\mu_3\text{-}Se)(\mu\text{-}SePh)_3(Ph)(\mu\text{-}dppm)]$ (**7**) with 50% probability thermal ellipsoids. Selected interatomic distances (Å) and angles (deg): Ru(1)···Ru(2) = 3.843, Ru(2)···Ru(3) = 3.872, Ru(1)···Ru(3) = 3.796, Ru(3)−P(1) = 2.351(3), Ru(1)−P(2) = 2.348(3), Ru(1)−Se(4) = 2.5516(16), Ru(1)−Se(1) = 2.5646(16), Ru(1)−Se(3) = 2.5916(16), Ru(2)−Se(1) = 2.5646(16), Ru(2)−Se(3) = 2.5689(16), Ru(2)−Se(2) = 2.6440(17), Ru(3)−Se(1) = 2.5539(16), Ru(3)−Se(4) = 2.5669(16), Ru(3)−Se(2) = 2.5810(16), Ru(2)−C(50) = 2.125(13); P(2)−C(15)−P(1) = 121.0(6), P(2)−Ru(1)−Se(4) = 93.95(9), Se(4)−Ru(1)−Se(1) = 82.32(5), Se(4)−Ru(1)−Se(3) = 85.15(5), Se(1)−Ru(1)−Se(3) = 83.07(5), Se(1)−Ru(2)−Se(3) = 83.52(5), Se(1)−Ru(2)−Se(2) = 82.13(5), Se(3)−Ru(2)−Se(2) = 93.71(5), Se(1)−Ru(3)−Se(4) = 82.23(5), Se(1)−Ru(3)−Se(2) = 83.59(5), Se(4)−Ru(3)−Se(2) = 77.96(5), Ru(3)−Se(1)−Ru(1) = 95.73(5), Ru(3)−Se(1)−Ru(2) = 98.32(5), Ru(1)−Se(1)−Ru(2) = 97.06(5), Ru(2)−Se(3)−Ru(1) = 96.27(5), Ru(3)−Se(2)−Ru(2) = 95.65(5), Ru(1)−Se(4)−Ru(3) = 95.73(5).

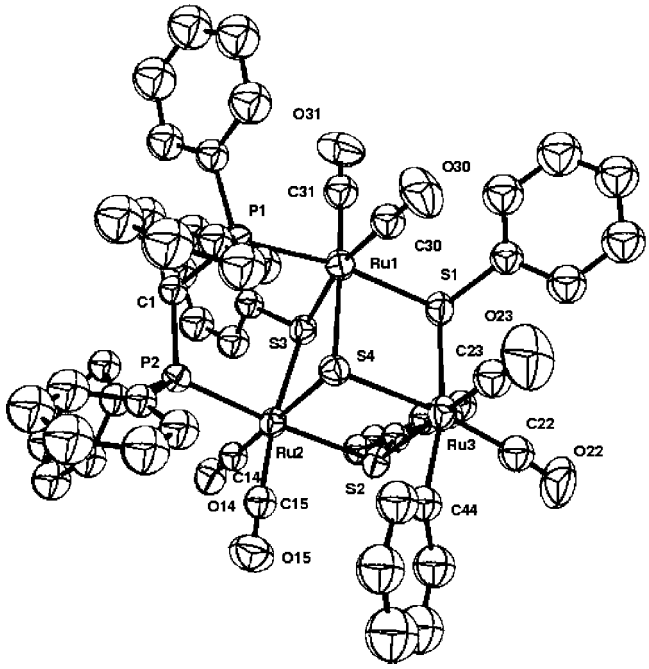

Figure 5. ORTEP diagram of $[Ru_3(CO)_6(\mu_3\text{-}S)(\mu\text{-}SPh)_3(Ph)(\mu\text{-}dppm)]$ (**10**) with 50% probability thermal ellipsoids. Selected interatomic distances (Å) and angles (deg): Ru(1)···Ru(6) = 3.670, Ru(2)···Ru(3) = 3.682, Ru(1)···Ru(3) = 3.723, Ru(1)−P(1) = 2.344(3), Ru(2)−P(2) = 2.348(3), Ru(2)−S(4) = 2.440(2), Ru(2)−S(2) = 2.480(2), Ru(3)−C(44) = 2.129(11), Ru(3)−S(4) = 2.451(2), Ru(3)−S(2) = 2.456(2), Ru(1)−S(4) = 2.428(3), Ru(1)−S(3) = 2.456(3), Ru(1)−S(1) = 2.473(3), Ru(2)−S(3) = 2.438(3), Ru(3)−S(1) = 2.540(3); P(1)−Ru(1)−S(4) = 87.42(10), S(4)−Ru(1)−S(3) = 80.91(9), S(4)−Ru(1)−S(1) = 82.95(10), S(3)−Ru(1)−S(1) = 79.24(8), S(3)−Ru(2)−S(4) = 81.03(9), S(3)−Ru(2)−S(2) = 85.91(9), S(4)−Ru(2)−S(2) = 82.79(8), S(4)−Ru(3)−S(2) = 83.04(8), S(4)−Ru(3)−S(1) = 81.11(9), S(2)−Ru(3)−S(1) = 92.02(9), Ru(1)−S(4)−Ru(2) = 97.87(9), Ru(1)−S(4)−Ru(3) = 99.46(10), Ru(2)−S(4)−Ru(3) = 97.67(8), Ru(2)−S(3)−Ru(1) = 97.16(9), Ru(1)−S(1)−Ru(3) = 95.92(10), Ru(3)−S(2)−Ru(2) = 96.50(8), P(2)−C(1)−P(1) = 119.4(5).

are very similar and exhibit two doublets (δ 22.2 and 19.9, J = 12.6 Hz for **7**; δ 25.9 and 23.9, J = 12.6 Hz for **10**) and a singlet (δ 20.2 for **7**; δ 23.5 for **10**) clearly indicating the presence of two isomers in solution (see below), one having equivalent ^{31}P nuclei which are nonequivalent in the other. Consistent with the ^{31}P NMR spectra, the aliphatic region of the ^{1}H NMR spectra show four sets of multiplets for the diastereotopic methylene protons (δ 4.12, 3.96, 3.86, and 3.40 for **7**; δ 4.76, 3.80, 3.44, and 3.21 for **10**), which are also attributed to the presence of two isomers in solution (Scheme 5).

Variable-Temperature NMR Studies of 3, 6, 7, and 10. The VT ^{31}P NMR spectra for compounds **3** and **6** are virtually identical. At the low -temperature limit of −80 °C compound **6** shows four ^{31}P NMR resonances: a singlet at 28.2 ppm, a doublet at 28.0 ppm (J_{P-P} = 32.2 Hz), a singlet at 27.0 ppm, and a doublet at 26.4 ppm (J_{P-P} = 32.2 Hz) with approximate relative intensity 1:2:2:2 (Figure 7). In the case of compound **3**, the ^{31}P NMR shows the same pattern with chemical shifts as follows: a singlet at 14.5 ppm, a doublet at 14.3 ppm (J_{P-P} = 34.8 Hz), a singlet at 13.8 ppm, and a doublet at 13.5 ppm (J_{P-P} = 34.8 Hz) with approximate relative intensity 1:2:2:2. In addition, a careful inspection of the baseline surrounding these main resonances reveals at least three additional doublets of very low intensity. As the temperature is increased, all of the resonances broaden and coalesce, until at room temperature two sharp singlets are observed at 27.8 and 27.4 ppm. Further heating of the solution to 100 °C resulted in no significant changes in the spectrum and the onset of decomposition. The weighted average chemical shift of the two singlets is 27.4 ppm at room temperature, while the weighted average chemical shift of the two doublets is 27.2 ppm. The former is in good agreement with the low-temperature data, while the latter is not. However, it should be borne in mind that two of the low-intensity doublets observed are at 30.2 and 31.2 ppm and these could contribute significantly at higher temperatures to the observed weighted average of the two major doublets of 27.8 ppm. It would appear that there are two sets of isomers: one that is symmetrical with respect to the dppm ligand (**A** an d**B** in Scheme 4) and two that are unsymmetrical with respect to the dppm ligand (**C** and **D** in Scheme 4). There is dynamic exchange within each set, but not across sets within the temperature range examined. We assign the isomers that are symmetrical with respect to the dppm ligand to conformational isomers, which differ with respect to the relative disposition of the phenyl groups on the μ-EPh ligands. In isomer **A** the phenyl groups are transoid, and in isomer **B** they are cisoid. The two μ-EPh groups in **A** are related by an axis of symmetry and those in **B** by a plane of symmetry; thus, neither isomer destroys the magnetic equivalence of the phosphorus atoms in the dppm ligand. As the temperature is increased, a wagging motion of the μ-EPh ligands could equilibrate **A** and **B**. We propose that the unsymmetrical isotopes **C** and **D** are equilibrated by an edge-to-edge migration involving the edge of the Ru triangle not bridged by the dppm ligand. This process would also equilibrate conformational isomers associated with the μ-EPh ligands, only two of which are shown in Scheme 4. The small doublets seen in the low-temperature limiting spectrum can be assigned to the additional conformational isomers associated with the μ-EPh ligands (i.e., both μ-EPh anti with respect to the dppm ligand, both μ-EPh syn with respect to the dppm ligand, and two with the μ-EPh transoid with respect to each other and syn or anti with respect to the dppm ligand). It seems reasonable to propose that equilibration of all of these isomers which are unsymmetrical with respect to the dppm ligand would take place by edge hopping across the longer edges (weaker bonds) of the Ru triangle, not bridged by the dppm ligand. It is interesting to note that only isomers of type **A** are observed in the solid-state structure of **3**, while in the case of complex **9** two doublets are observed in the low-temperature limiting spectrum at 31.2 and 28.5 ppm (J_{P-P} = 30.3 Hz) at −80 °C in a relative intensity of 1:1 along with two additional tiny doublets at 34.0 and 29.7 ppm (J_{P-P} = 31.3 Hz), suggesting that only unsymmetrical isomers related to **C** and **D** (Scheme 4) are populated in solution. At room temperature these doublets average to a singlet at 31.2 ppm, indicating the same fluxional process is operative for **9** as for the **C** and **D** isomers in **3** and **6**. As for **3**, the minor isomers are contributing to the temperature-averaged chemical shift. That only the most symmetrical isomer **A** is observed for **3** in the solid state can be attributed to crystal-packing effects, while the greater stability of isomers related to **C** and **D** in the case of **9** in solution is probably the result of the smaller sulfur atom preferring to bridge the shorter dppm-bridged edge of the Ru triangle in the case of one of the μ-EPh ligands. That all four isomers equilibrate in solution by dissolving a pure sample of **3a** means that although **3a** and **3b** can be equilibrated on the

(25) Coleman, J. P.; Jones, D. F.; Dixneuf, P. H.; Brisson, C.; Bonnet, J.-J.; Lavigne, G. *Inorg. Chem.* **1984**, *23*, 952.

Scheme 3

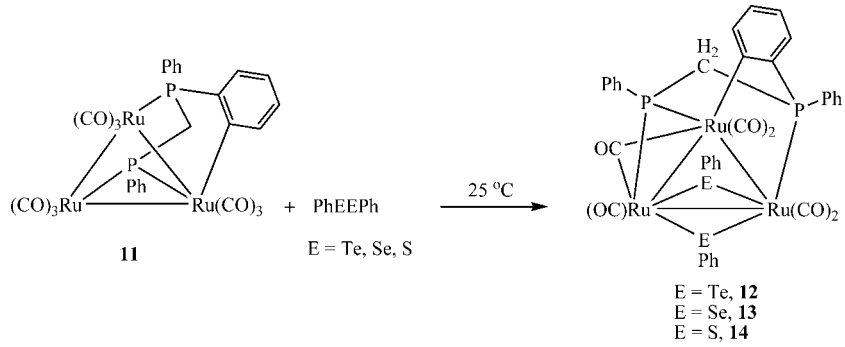

NMR time scale (milliseconds to seconds in this case) the formation of **3c** (or **3d**) takes place at a much slower rate not accessible on the NMR time scale up to 100 °C, but rapidly enough to form at ambient temperatures over the longer time scales associated with dissolution and standing in solution over the course of hours.

Compound **7** shows the presence of two isomers in solution, as evidenced by the presence of two doublets at 26.9 and 24.9 ppm (J_{P-P} = 12.6 Hz) and a singlet at 24.3 ppm with relative intensities of 1:1:3 (Figure 8). As the temperature is increased to 100 °C, the doublet at 24.9 ppm and the singlet at 24.3 ppm begin to broaden. Further increases in temperature were limited by the solvent and the onset of slow decomposition of the cluster. Compound **7** is apparently a very rigid molecule, and we assign the minor changes in the spectrum to the onset of axial radial exchange on the phenyl-substituted ruthenium atom (Scheme 5). Compound **10** shows similar behavior.

Reactions of $[Ru_3(CO)_9\{\mu_3\text{-}\eta^3\text{-}P(C_6H_5)CH_2P(C_6H_5)\text{-}(C_6H_4)\}]$ (11) with PhEEPh (E = Te, Se, S). The new compounds $[Ru_3(CO)_6(\mu\text{-}EPh)_2\{\mu_3\text{-}\eta^3\text{-}P(C_6H_5)CH_2P(C_6H_5)\text{-}(C_6H_4)\}]$ (E = Te, **12**, 24%; E = Se, **13**, 28%; E = S, **14**, 28%) were obtained as the only products from the reactions of the ortho-metalated compound **11** with PhEEPh in refluxing THF (Scheme 3). Compounds **12–14** were characterized by a combination of elemental analysis, IR, ^{1}H NMR, ^{31}P{^{1}H} NMR, and mass spectral data as well as single-crystal X-ray diffraction analysis of one of the representative compounds, **13**.

An ORTEP diagram of the molecular structure of **13** is shown in Figure 6, crystal data are given in Table 1, and selected bond distances and angles are collected in the caption to the figure. The molecule consists of a triangular cluster of ruthenium atoms with two bridging SePh ligands, a triply bridging $PhPCH_2P\text{-}(C_6H_4)Ph$ ligand, five terminal carbonyl ligands, and a semibridging carbonyl ligand. The Ru_3 triangle is significantly distorted and has one long bond (Ru(1)−Ru(3) = 3.0566(4) Å) one significantly short bond (Ru(1)−Ru(2) = 2.7470(4) Å), and one fairly short bond, (Ru(2)−Ru(3) = 2.7909(4) Å). The

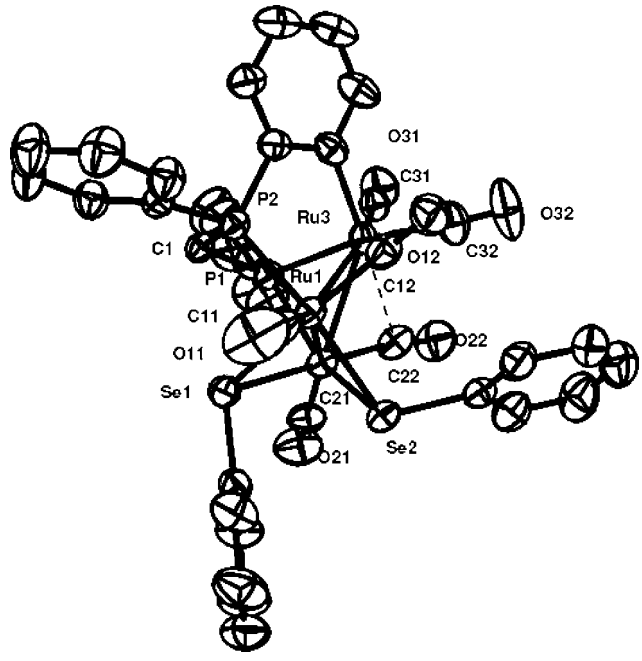

Figure 6. ORTEP diagram of $Ru_3(CO)_5(\mu\text{-}CO)(\mu\text{-}SePh)_2\text{-}\{PhPCH_2P(C_6H_4)Ph\}]$ (**13**) with 50% probability thermal ellipsoids. Selected interatomic distances (Å) and angles (deg): Ru(1)−Ru(2) = 2.7470(4), Ru(1)−Ru(3) = 3.0566(4), Ru(2)−Ru(3) = 2.7909(4), Ru(1)−Se(1) = 2.5504(5), Ru(2)−Se(1) = 2.5049(5), Ru(1)−Se(2) = 2.5322(5), Ru(2)−Se(2) = 2.5297(5), Ru(2)−C(22) = 1.907(5), Ru(3)−C(22) = 2.579(4), Ru(2)−P(1) = 2.3209(10), Ru(1)−P(2) = 2.3334(9), Ru(3)−P(1) = 2.3044(10); Ru(1)−Ru(2)−Ru(3) = 66.995(11), Ru(2)−Ru(1)−Ru(3) = 57.189(11), Ru(2)−Ru(3)−Ru(1) = 55.816(10), Ru(2)−Se(1)−Ru(1) = 65.822(14), Ru(2)−Se(2)−Ru(1) = 65.733(13), Se(1)−Ru(2)−Ru(1) = 57.887(13), Se(2)−Ru(2)−Ru(1) = 57.178(12), Se(1)−Ru(2)−Ru(3) = 113.881(16), Se(2)−Ru(2)−Ru(3) = 100.137(15), Se(1)−Ru(1)−Ru(2) = 56.290(13), Se(2)−Ru(1)−Ru(2) = 57.089(13), Se(1)−Ru(1)−Ru(3) = 104.396(15), Se(2)−Ru(1)−Ru(3) = 93.403(14), Ru(2)−C(22)−Ru(3) = 75.28(14), C(41)−P(1)−C(1) = 106.76(18), P(1)−C(1)−P(2) = 103.00(18), P(1)−Ru(3)−Ru(1) = 77.96(3), P(1)−Ru(3)−Ru(2) = 53.16(3), P(1)−Ru(2)−Ru(3) = 52.62(3), P(2)−Ru(1)−Ru(3) = 70.97(3).

Scheme 4

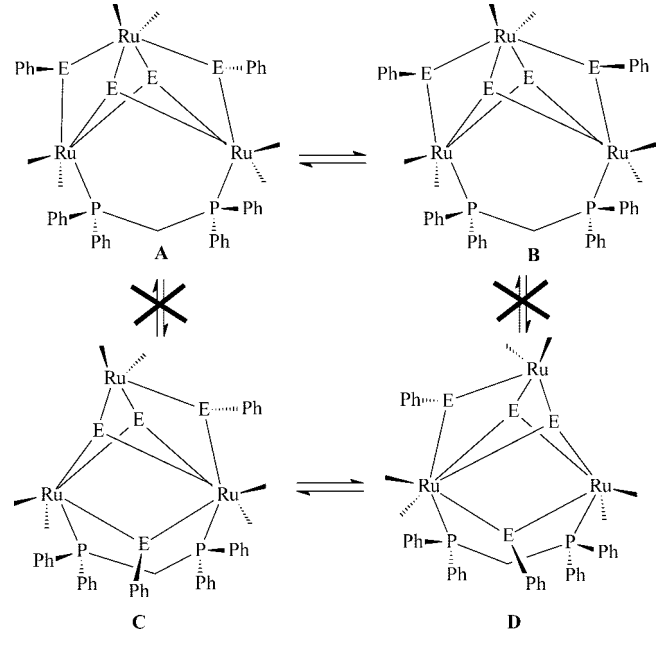

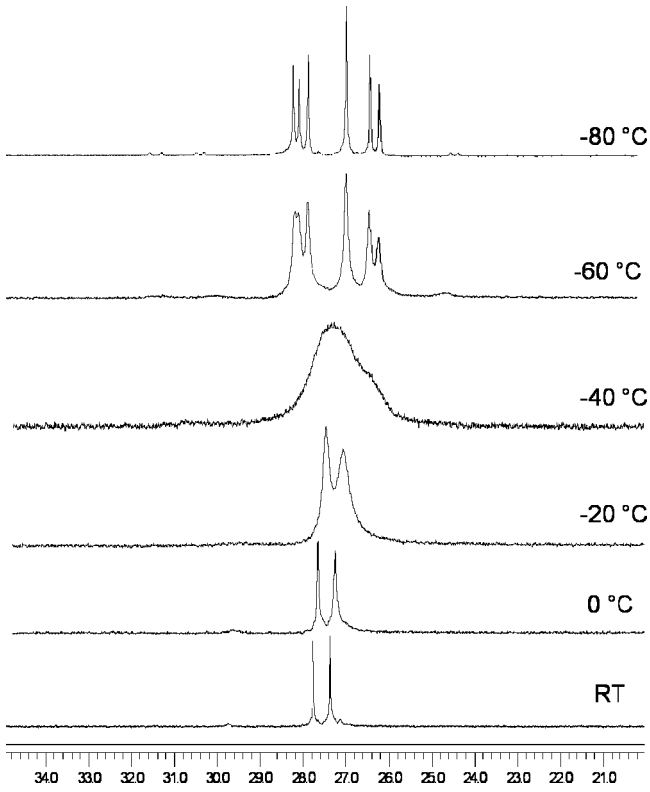

Figure 7. VT $^{31}P\{^1H\}$ NMR spectra of $[Ru_3(CO)_6(\mu_3\text{-}Se)_2(\mu\text{-}SePh)_2(\mu\text{-}dppm)]$ (**6**) in CD_2Cl_2.

Scheme 5

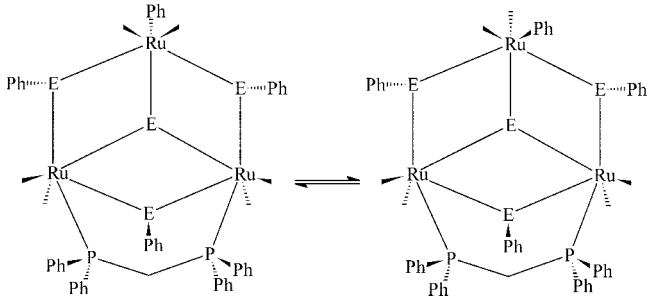

last one is also shorter than the average Ru−Ru distances in $[Ru_3(CO)_{12}]$ (2.8564(10) Å).[26] An intriguing feature of the structure is the occurrence of two of the phenylselenido ligands across the same Ru(1)−Ru(2) vector. The shortening of this ruthenium−ruthenium bond is most probably due to the "pincer" effect exerted by the bridging SePh ligands rather than the strength of the metal−metal interaction. It is remarkable that one SePh ligand asymmetrically bridges the Ru(1)−Ru(2) edge (Ru(2)−Se(1) = 2.5049(5) and Ru(1)−Se(1) = 2.5504(5) Å) while the other bridges symmetrically (Ru(1)−Se(2) = 2.5322(5) Å and Ru(2)−Se(2) = 2.5297(5) Å). Among the six carbonyl ligands attached to the metals of the skeleton, one carbonyl (C(22)−O(22)) is semibridging to the Ru(3) atom (Ru(3)−C(22) = 2.579(4) and Ru(2)−C(22) = 1.907(5) Å) with Ru(3)−C(22)−O(22) and Ru(2)−C(22)−O(22) angles of 117.4(4) and 166.8(4)°, respectively, and the α value of 0.35 supports the description of C(22)−O(22) as semibridging.[27] The bonding mode of the ortho-metalated $PhPCH_2P(C_6H_4)Ph$ ligand bears a strong resemblance to that of the starting compound **11**.[28] One of the phosphorus atoms, P(1), asymmetrically bridges the Ru(3)−Ru(2) edge (Ru(2)−P(1) = 2.3209(10) and Ru(3)−P(1) = 2.3044(10) Å), while P(2) is coordinated to Ru(1) (Ru(1)−P(2) = 2.3334(9) Å). The compound contains 48 valence electrons and is electron precise with three metal−metal bonds.[23]

The spectroscopic data of **13** are consistent with the solid-state structure, and the spectroscopic data of **12** and **14** indicate that they are isostructural. The patterns of the carbonyl stretching frequencies in the IR spectra of **12**−**14** are very similar, indicating that they have very similar distributions of the carbonyl ligands. In addition to the phenyl proton resonance of the dppm and TePh moieties in the aromatic region, the ^1H NMR spectra exhibit well-separated signals for the ortho-metalated phenyl group and the methylene protons of the dppm ligand. The $^{31}P\{^1H\}$ NMR spectra of **12**–**14** exhibit two doublets (δ 67.5 and 1.0, J_{P-P} = 55.1 Hz for **12**; δ 86.8 and 4.0, J_{P-P} = 54.3 Hz for **13**; δ 85.6 and 4.6, J_{P-P} = 51.3 Hz for **14**) consistent with their structures. Their mass spectra confirm the stoichiometry with molecular ion peaks (*m*/*z* 1188 for **12**, *m*/*z* 1090 for **13**, and *m*/*z* 997 for **14**).

Conclusions

The work presented here demonstrates that the dppm-bridged triruthenium cluster **1** exhibits high reactivity toward diphenyl dichalcogenides at room temperature, which often leads to metal−metal bond cleavage. Not only can EPh groups, formed by facile cleavage of E−E bonds, be inserted into the Ru−Ru bond but also capping chalcogenido ligands are formed by further cleavage of E−C bonds. Furthermore, in contrast to the reactions of the parent dodecacarbonyl, which furnished only dinuclear compounds, and to $[Os_3(CO)_{10}(\mu\text{-dppm})]$, which afforded the di- and trinuclear complexes given in Chart 1 when treated with PhEEPh, the reactions of **1** with PhEEPh (E = Te, Se, S) gave clusters with all three Ru−Ru bonds opened, containing bridging EPh groups and capping chalcogenido ligands, in spite of the presence of the bridging dppm ligand. Notably, the osmium analogues of compounds **3**, **4**, **6**, **7**, **9**, and **10** were not detected from the reactions of $[Os_3(CO)_{10}(\mu\text{-dppm})]$ with PhEEPh, even under forcing reaction conditions. This is probably due to the relatively high lability of the ruthenium clusters compared with that of osmium. The ortho-metalated compound **11** has been shown to react with PhEEPh through oxidative cleavage of the E−E bond by adding both EPh moieties across the unbridged Ru−Ru edge of the cluster. Most likely, the capping $\mu_3\text{-}\eta^3\text{-}P(C_6H_5)CH_2P(C_6H_5)(C_6H_4)$ ligand in **12**–**14** helps to keep the metal triangle intact. It would appear that the relative stability of the isomers of compounds **3**, **6**, and **9** in solution and their ability to interconvert is governed by the size of the chalcogenide atom as it relates to the strength of the μ-EPh bridge. Finally, the unusual chalcogen-rich 54-electron compounds **3**, **4**, **6**, **7**, **9**, and **10** reported in this study should be useful precursors for the preparation of solid-state materials.

Experimental Section

All reactions and manipulations were carried out under an atmosphere of prepurified nitrogen by using standard Schlenk techniques. All solvents were purified by distillation from an appropriate drying agent. Infrared spectra were recorded on a

(26) Churchill, M. R.; Hollander, F. J.; Hatchinson, J. P. *Inorg. Chem.* **1977**, *16*, 2655.

(27) Curtis, M. D.; Han, K. R.; Butler, W. M. *Inorg. Chem.* **1980**, *19*, 2096.

(28) Lugan, N.; Bonnet, J. J.; Ibers, J. A. *J. Am. Chem. Soc.* **1985**, *107*, 4484.

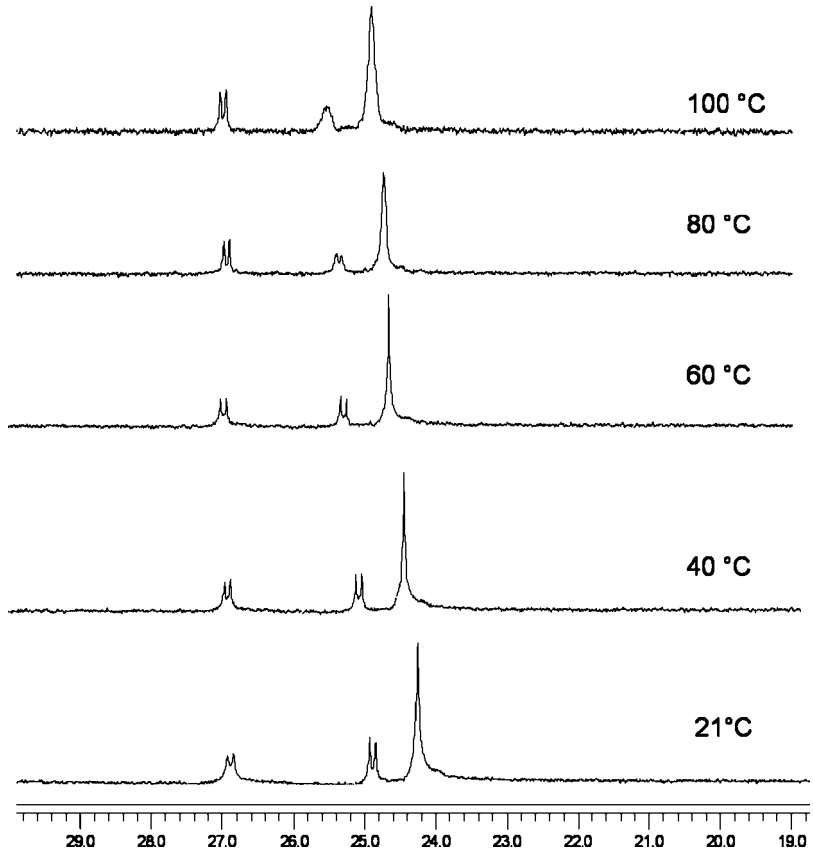

Figure 8. VT $^{31}P\{^1H\}$ NMR spectra of $[Ru_3(CO)_6(\mu_3\text{-Se})(\mu\text{-SePh})_3(Ph)(\mu\text{-dppm})]$ (**7**) in CD_2Cl_2.

Shimadzu FTIR 8101 spectrophotometer. NMR spectra were recorded on a Bruker DPX 400 spectrometer. Chemical shifts for the $^{31}P\{^1H\}$ NMR spectra are relative to 85% H_3PO_4. The starting clusters $[Ru_3(CO)_{10}(\mu\text{-dppm})]$[29] and $[Ru_3(CO)_9\{\mu_3\text{-}\eta^3\text{-}P(C_6H_5)\text{-}CH_2P(C_6H_5)(C_6H_4)\}]$[28] were prepared according to the published procedures.

Reaction of $[Ru_3(CO)_{10}(\mu\text{-dppm})]$ (1) with PhTeTePh. A CH_2Cl_2 solution (30 mL) of **1** (205 mg, 0.212 mmol) and PhTeTePh (174 mg, 0.425 mmol) was stirred at room temperature for 72 h. The solvent was removed under reduced pressure and the residue chromatographed by TLC on silica gel. Elution with cyclohexane/CH_2Cl_2 (1/1, v/v) developed three bands, which afforded the following three compounds, in order of elution: $[Ru_2(CO)_4(\mu\text{-TePh})_2(\mu\text{-dppm})]$ (**2**; 33 mg, 14%) as orange crystals from hexane/CH_2Cl_2 at −4 °C, $[Ru_3(CO)_6(\mu_3\text{-Te})_2(\mu\text{-TePh})_2(\mu\text{-dppm})]$ (**3**; 58 mg, 18%) as red crystals, and $[Ru_3(CO)_6(\mu_3\text{-Te})(\mu\text{-TePh})_3(COPh)(\mu\text{-dppm})]$ (**4**; 81 mg, 22%) as red crystals after recrystallization from hexane/CH_2Cl_2 at −20 °C. Spectral data for **2**: IR (ν(CO), CH_2Cl_2) 1999 s, 1973 vs, 1937 s cm^{-1}; ^1H NMR (CD_2Cl_2) δ 7.74–7.01 (m, 30H), 4.57 (m, 1H), 4.29 (m, 1H); $^{31}P\{^1H\}$ NMR (CD_2Cl_2) δ 13.9 (s); mass spectrum *m*/*z* 1108. Anal. Calcd for $C_{41}H_{32}O_4P_2Ru_2Te_2$: C, 44.44; H, 2.91. Found: C, 44.46; H, 3.01. Spectral data for **3**: IR (ν(CO), CH_2Cl_2) 2021 vs, 2010 vs, 1970 vs, 1953 m cm^{-1}; ^1H NMR (CD_2Cl_2) δ 8.15–7.03 (m, 30H), 4.07 (m, 2H); $^{31}P\{^1H\}$ NMR (CD_2Cl_2, −80 °C) δ 14.5 (s), 14.3 (d, J_{P-P} = 34.8 Hz), 13.8 (s), 13.5 (d, J_{P-P} = 34.8 Hz); FAB mass spectrum *m*/*z* 1522. Anal. Calcd for $C_{43}H_{32}O_6P_2Ru_3Te_4$: C, 33.97; H, 2.12. Found: C, 34.06; H, 2.17. Spectral data for **4**: IR (ν(CO), CH_2Cl_2) 2022 vs, 2004 s, 1972 s, 1945 m cm^{-1}; IR (ν(CO), KBr) 1735 s cm^{-1}; ^1H NMR (CD_2Cl_2) δ 7.93 (d, 1H, J = 7.4 Hz), 7.85 (d, 1H, J = 7.2 Hz), 7.71 (d, 1H, J = 7.2 Hz), 7.65 (d, 1H, J = 7.2 Hz), 7.57 (dd, 1H, J = 7.2, 3.2 Hz), 7.48–6.83 (m, 35H), 4.12 (t, 2H, J = 12.4 Hz); $^{31}P\{^1H\}$ NMR (CD_2Cl_2) δ 12.1(J_{P-P} = 11.7 Hz), 11.1 (d, J_{P-P} = 11.7 Hz); FAB mass spectrum *m*/*z* 1704. Anal. Calcd for $C_{56}H_{42}O_7P_2Ru_3Te_4$: C, 39.51; H, 2.49. Found: C, 39.68; H, 2.58.

Reaction of 1 with PhSeSePh. A reaction similar to that above of **1** (200 mg, 0.207 mmol) with PhSeSePh (129 mg, 0.413 mmol) in THF (35 mL) followed by similar chromatographic separation afforded the following compounds, in order of elution: $[Ru_2(CO)_4(\mu\text{-SePh})_2(\mu\text{-dppm})]$ (**5**; 22 mg, 11%), $[Ru_3(CO)_6(\mu_3\text{-Se})_2(\mu\text{-SePh})_2(\mu\text{-dppm})]$ (**6**; 69 mg, 25%), and $[Ru_3(CO)_6(\mu_3\text{-Se})(\mu\text{-SePh})_3(Ph)(\mu\text{-dppm})]$ (**7**; 107 mg, 35%) as yellow crystals after recrystallization from hexane/CH_2Cl_2 by slow evaporation of the solvents at −4 °C. Spectral data for **5**: IR (ν(CO), CH_2Cl_2) 2004 vs, 1981 vs, 1942 s cm^{-1}; ^1H NMR (CD_2Cl_2) δ 7.69–7.09 (m, 30H), 4.42 (m, 1H), 3.87 (m, 1H); $^{31}P\{^1H\}$ NMR (CD_2Cl_2) δ 24.2 (s); FAB mass spectrum *m*/*z* 1012. Anal. Calcd for $C_{41}H_{32}O_4P_2Ru_2Se_2$: C, 48.72; H, 3.19. Found: C, 48.78; H, 3.25. Spectral data for **6**: IR (ν(CO), CH_2Cl_2) 2031 vs, 2020 s, 1975 s, 1958 m cm^{-1}; ^1H NMR (CD_2Cl_2) δ 8.28–8.23 (m, 5H), 7.45 (br, 10H), 7.26–7.10 (m, 15H), 3.73 (m, 2H); $^{31}P\{^1H\}$ NMR (CD_2Cl_2, −80 °C) δ 28.2 (s), 28.0 (d, J_{P-P} = 32.2 Hz), 27.0 (s), 26.4 (d, J_{P-P} = 32.2 Hz); FAB mass spectrum *m*/*z* 1326. Anal. Calcd for $C_{43}H_{32}O_6P_2Ru_3Se_4$: C, 38.96; H, 2.43. Found: C, 39.11; H, 2.59. Spectral data for **7**: IR (ν(CO), CH_2Cl_2) 2033 vs, 2010 s, 1978 s, 1947 m cm^{-1}; ^1H NMR (CD_2Cl_2) δ 8.03–6.88 (m, 40 H), 4.12 (m, 1H), 3.96 (m, 1H), 3.86 (m, 1H), 3.40 (m, 1H); $^{31}P\{^1H\}$ NMR (toluene-d_8) δ 26.9 (d, J_{P-P} = 12.6 Hz), 24.3 (s), 24.9 (d, J_{P-P} = 12.6 Hz); FAB mass spectrum *m*/*z* 1480. Anal. Calcd for $C_{55}H_{42}O_6P_2Ru_3Se_4$: C, 44.64; H, 2.86. Found: C, 44.69; H, 2.90.

Reaction of 1 with PhSSPh. A reaction similar to that above between **1** (200 mg, 0.207 mmol) and PhSSPh (90 mg, 0.413 mmol) in THF (35 mL) followed by similar chromatographic separation developed five bands. The first three bands afforded, in order of elution, $[Ru_2(CO)_4(\mu\text{-SPh})_2(\mu\text{-dppm})]$ (**8**; 28 mg, 15%) and $[Ru_3(CO)_6(\mu_3\text{-S})_2(\mu\text{-SPh})_2(\mu\text{-dppm})]$ (**9**; 42 mg, 18%) as yellow crystals and $[Ru_3(CO)_6(\mu_3\text{-S})(\mu\text{-SPh})_3(Ph)(\mu\text{-dppm})]$ (**10**; 38 mg,

(29) Bruce, M. I.; Nicholson, B. K.; Williams, M. L. *Inorg. Synth.* **1990**, *26*, 265.

14%) as orange crystals after recrystallization from hexane/CH_2Cl_2 at −4 °C. Spectral data for **8**: IR (ν(CO), CH_2Cl_2) 2006 s, 1983 vs, 1945 s cm^{-1}; ^1H NMR (CD_2Cl_2) δ 7.67–7.63 (m, 3H), 7.50–7.44 (m, 5H), 7.38–7.26 (m, 8H), 7.16–7.02 (m, 4H), 4.34 (m, 1H), 3.59 (m, 1H); $^{31}P\{^1H\}$ NMR (CD_2Cl_2) δ 29.3 (s); FAB mass spectrum *m*/*z* 918. Anal. Calcd for $C_{41}H_{32}O_4P_2Ru_2S_2$: C, 53.71; H, 3.52. Found: C, 53.75; H, 3.58. Spectral data for **9**: IR (ν(CO), CH_2Cl_2) 2027 s, 2008 vs, 1989 vs, 1954 vs cm^{-1}; ^1H NMR (CD_2Cl_2) δ 7.88 (d, J = 7.2 Hz, 2H), 7.65 (m, 2H), 7.48 (m, 2H), 7.39–7.29 (m, 18H), 7.21 (m, 2H), 7.10 (m, 2H), 7.01 (m, 2H), 4.28 (m, 1H), 3.76 (m, 1H); $^{31}P\{^1H\}$ NMR ($CDCl_2$, −80 °C) δ 31.2 (J_{P-P} = 30.3 Hz), 28.5 (J_{P-P} = 30.3 Hz), 34.0 (J_{P-P} = 31.3 Hz), 29.7 (J_{P-P} = 31.3 Hz); FAB mass spectrum *m*/*z* 1139. Anal. Calcd for $C_{43}H_{32}O_6P_2Ru_3S_4$: C, 45.38; H, 2.83. Found: C, 45.46; H, 2.80. Spectral data for **10**: IR (ν(CO), CH_2Cl_2): 2041 vs, 2014 s, 1985 s, 1946 m cm^{-1}; ^1H NMR (CD_2Cl_2) δ 7.99–6.73 (m, 40 H), 4.76 (m, 1H), 3.80 (m, 1H), 3.44 (m, 1H), 3.21(m, 1H); $^{31}P\{^1H\}$ NMR (toluene-d_8) δ 25.9 (d, J_{P-P} = 12.6 Hz), 23.9 (d, J_{P-P} = 12.6 Hz), 23.5 (s); FAB mass spectrum *m*/*z* 1293. Anal. Calcd for $C_{55}H_{42}O_6P_2Ru_3S_4$: C, 51.12; H, 3.28. Found: C, 51.16; H, 3.33.

Reactions of $[Ru_3(CO)_9\{\mu_3\text{-}\eta^3\text{-}P(C_6H_5)CH_2P(C_6H_5)(C_6H_4)\}]$ (11) with PhEEPh (E = Te, Se, S). To a THF solution (25 mL) of **11** (80 mg, 0.093 mmol) was added 2 equiv of PhEEPh, and the reaction mixture was heated to reflux for 2–6 h. The solvent was removed under reduced pressure and the residue chromatographed by TLC on silica gel. Elution with hexane/CH_2Cl_2 (2/1, v/v) developed two bands. The first band gave unreacted **11** (∼10 mg), while the second band afforded $[Ru_3(CO)_5(\mu\text{-EPh})_2(\mu\text{-CO})\{\mu_3\text{-}\eta^3\text{-}PPhCH_2PPh(C_6H_4)\}]$ (**12**, E = Te, 26 mg, 24%; **13**, E = Se, 28 mg, 28%; **14**, E = S, 26 mg, 28%) as red crystals from hexane/CH_2Cl_2 at −5 °C. Spectral data for **12**: IR (ν(CO), CH_2Cl_2) 2031 s, 2002 vs, 1985 vs, 1967 m, 1952 m, 1925 w cm^{-1}; ^1H NMR (CD_2Cl_2) δ 7.77–7.06 (m, 21H), 6.82 (m, 1H), 6.56 (m, 1H), 6.10 (m, 1H), 4.90 (m, 1H), 4.49 (m, 1H).; $^{31}P\{^1H\}$ NMR (CD_2Cl_2) δ 67.5 (d, J_{P-P} = 55.1 Hz), 1.0 (d, J_{P-P} = 55.1 Hz); FAB mass spectrum *m*/*z* 1188. Anal. Calcd for $C_{37}H_{26}O_6P_2Ru_3Te_2$: C, 37.44; H, 2.21. Found: C, 37.47; H, 2.19. Spectral data for **13**: IR (ν(CO), CH_2Cl_2) 2035 vs, 2010 vs, 1991 vs, 1970 w, 1954 s, 1931 w cm^{-1}; ^1H NMR (CD_2Cl_2) δ 7.43 (m, 21H), 6.88 (m, 1H), 6.74 (m, 1H), 6.15 (m, 1H), 4.57 (m, 1H), 3.86 (m, 1H); $^{31}P\{^1H\}$ NMR (CD_2Cl_2) δ 86.8 (d, J_{P-P} = 54.3 Hz), 4.0 (d, J_{P-P} = 54.3 Hz); FAB MS *m*/*z* 1090. Anal. Calcd for $C_{37}H_{26}O_6P_2Ru_3Se_2$: C, 40.78; H, 2.40. Found: C, 41.82; H, 2.46. Spectral data for **14**: IR (ν(CO), CH_2Cl_2) 2030 vs, 2011 vs, 1993 vs, 1954 s, 1931 w cm^{-1}; ^1H NMR (CD_2Cl_2) δ 7.45 (m, 21H), 6.85 (m, 1H), 6.17 (m, 1H), 6.12 (m, 1H), 4.53 (m, 1H), 3.88 (m, 1H); $^{31}P\{^1H\}$ NMR (CD_2Cl_2) δ 85.6 (d, J_{P-P} = 51.3 Hz), 4.6 (d, J_{P-P} = 51.3); FAB mass spectrum *m*/*z* 997. Anal. Calcd for $C_{37}H_{26}O_6P_2Ru_3S_2$: C, 44.62; H, 2.63. Found: C, 44.67; H, 2.69.

X-ray Structure Determination of 2−4, 7, and 10. Crystals of **2**−**4**, **7**, and **10** for X-ray structural determination were obtained from saturated solutions of each in hexane/dichloromethane solvent at −20 °C. Crystallographic data for compounds **2**−**4**, **7**, and **10** were collected at 296 K with Mo Kα radiation (λ = 0.710 73 Å). Data collection and processing were carried out using XSCANS.[30] The unit cells were indexed on low-angle reflections and refined from 25 reflections in a range of 12–13°. The structures were solved by direct methods (SHELXS-97)[31] and refined on F^2 by full-matrix least squares (SHELXL-97),[32] utilized as incorporated in the WINGX[33] program package using all unique data. All non-hydrogen atoms were refined anisotropically for all structures except **9**, for which all carbon atom thermal parameters were refined isotropically. Hydrogen atoms were included in calculated positions (riding model) with the U_{iso} value set at 1.2 times the U_{eq} value of the parent atom. Initially for all the crystals, data collection was set to 50° (2θ). During the data collection process it became evident that, as some of the crystals diffracted poorly, therefore the data collection was set to a smaller 2θ. Because of this, "completeness to theta" values for **3**, **7**, and **9** were 53.2%, 72.2% and 55.2%, respectively. Crystallographic and other experimental data are summarized in Table 1.

X-ray Structure Determination of 13. Single crystals of compound **13** were mounted on glass fibers, and all geometric intensity data were obtained from these samples on a Bruker SMART APEX CCD diffractometer using graphite-monochromated Mo Kα radiation (λ= 0.710 73 Å) at 150 ± 2 K. Data reduction and integration were carried out with SAINT+ and absorption corrections applied using the program SADABS.[34] Structures were solved by direct methods and developed using alternating cycles of least-squares refinement and difference-Fourier synthesis. All non-hydrogen atoms were refined anisotropically. Hydrogen atoms were placed in calculated positions and their thermal parameters linked to those of the atoms to which they were attached (riding model). The SHELXTL PLUS V6.10 program package was used for the structure solution and refinement.[34]

Crystallographic data for the structural analyses have been deposited with the Cambridge Crystallographic Data Centre: CCDC Nos. 251653 for **2**, 251654 for **3**, 251655 for **4**, 251656 for **7**, 251653 for **10**, and 259011 for **13**. Copies of this information may be obtained free of charge from The Director, CCDC, 12 Union Road Cambridge CB2 1EZ, U.K. (fax, +44-1223-336033; email, deposit@ccdc.cam.ac.uk; web, http://www.ccdc.cam.ac.uk).

Acknowledgment. We thank Professor A. J. Deeming (Department of Chemistry, University College London) for obtaining X-ray data on compound **13**. N.B. acknowledges Sher-e-Bangla Agricultural University, for study leave.

Supporting Information Available: CIF files giving crystallographic data for **2**−**4**, **7**, **10**, and **13**. This material is available free of charge via the Internet at http://pubs.acs.org.

OM701042S

(30) XSCANS: Data Collection Software, Release 2.10b; Bruker AXS Inc., Madison, WI, 1994.
(31) Sheldrick, G. M. *Acta Crystallogr.* **1990**, *46*, 467.
(32) Sheldrick, G. M. SHELXL-97: Program for Crystal Structure Refinement; University of Gottingen, Gottingen, Germany, 1997.
(33) Farrugia, L. J. *J. Appl. Crystallogr.* **1999**, *32*, 837.
(34) SMART and SAINT Software for CCD Diffractometers, Version 6.1; Bruker AXS Inc., Madison, WI, 2000.